

Original Research

# Preparation and Characterization of Allicin-Loaded Solid Lipid Nanoparticles Surface-Functionalized with Folic Acid-Bonded Chitosan: *In Vitro* Anticancer and Antioxidant Activities

Faris J. Alyasiri<sup>1</sup> , Maryam Ghobeh<sup>1</sup> , Masoud Homayouni Tabrizi<sup>2,\*</sup> <sup>1</sup>Department of Biology, Science and Research Branch, Islamic Azad University, 1477893855 Tehran, Iran<sup>2</sup>Department of Biology, Mashhad Branch, Islamic Azad University, 91735 Mashhad, Iran\*Correspondence: [mhomayouni6@gmail.com](mailto:mhomayouni6@gmail.com); [mhomayouni6@mshdiau.ac.ir](mailto:mhomayouni6@mshdiau.ac.ir) (Masoud Homayouni Tabrizi)

Academic Editor: Roberto Bei

Submitted: 21 December 2022 Revised: 24 May 2023 Accepted: 8 June 2023 Published: 13 July 2023

## Abstract

**Objective:** This investigation aimed to increase the bioavailability and anticancer effects of allicin (AC) by encapsulating it in solid lipid nanoparticles (SLN) decorated with chitosan (CS)-conjugated folic acid (FA). **Material and Methods:** Nanoparticles (NPs) were synthesized by high-pressure homogenization, and then, Fourier-transform infrared (FTIR), Field-Emission Scanning Electron Microscopy (FESEM), Dynamic Light Scattering (DLS), and zeta potential methods were used to determine their physicochemical characteristics. 3-(4,5-dimethylthiazol-2-yl)-2,5-diphenyltetrazolium bromide (MTT) assay was performed to assess the effect of toxicity and flow cytometry, while fluorescent staining methods were used to investigate the type of cell death. Real-time quantitative polymerase chain reaction (qPCR) was used to evaluate the expression levels of apoptotic genes: *Bcl-2*, and *caspase-8*. **Results:** The presence of AC-SLN-CS-FA with a spherical morphology, an average size of  $86.7 \pm 9.4$  nm, uniform distribution (0.31), a surface charge of  $+21.3 \pm 13.3$  mV, an encapsulation percentage of 86.3%, and a folate binding rate of 63% confirmed the success of the preparation method. Suppression of MCF-7 cancer cells and non-toxicity of AC-SLN-CS-FA on Human foreskin fibroblast (HFF) normal cells were confirmed by cytotoxic assay. The results of flow cytometry revealed that the cells were arrested in the sub-G1 phase, and the activation of the intrinsic apoptosis pathway was confirmed by the results of real-time qPCR. **Conclusions:** In general, AC-SLN-CS-FA has the potential to prevent free radicals and trigger apoptosis in cancer cells by activating the intrinsic apoptosis pathway; thus, making it a promising subject in preclinical research.

**Keywords:** BAX; solid lipid nanocarrier; allicin; chitosan; anticancer; encapsulation

## 1. Introduction

Genetic instability and mutations in genes involved in cell proliferation, including proto-oncogenes, tumor suppressor genes, etc., can increase cell proliferation, inhibit apoptosis, and cause malignancy in cells [1]. The identification of cellular and molecular processes involved in the development of various diseases, including cancer, has led to the achievement and development of therapeutic molecules with the ability to affect target tissues [2]. Presently, herbal bioactive compounds receive much attention because of their extensive biological effects and fewer side effects compared to chemotherapy [3,4].

Allicin (AC), an organosulfur compound found in garlic, has anticancer, antioxidant, anti-inflammation, and antibacterial effects, which have been reported in many investigations [5]. However, the insolubility and entrapment of this compound in plasma membrane proteins and fatty acids have limited its clinical application [6]. The use of nano-based drug delivery systems (NDDSs), which possess the ability to protect the drug against degradation and control its release, can be an effective step to remove such restrictions [3,7,8].

Solid lipid nanoparticles (SLNs) are excellent carriers for loading hydrophobic compounds [9–11]. These NPs consist of a lipid matrix core encircled by a layer, the structure of which allows the hydrophobic compounds to be loaded into the core of the NPs, with high efficiency [12]. The non-toxicity and stability of SLNs represent their main advantages compared to polymeric and lipid NPs [13,14]. Drug loading in these NDDSs, while protecting them against proteolytic degradation, also leads to a controlled release and targeted drug delivery [15–17]. These carriers are limited only by the lack of control over drug release under systemic conditions [18] and their anionic nature, which allows for its rapid detection and disposal through the reticuloendothelial system (RES) [19]. Decorating the surface of NPs with polymers, such as chitosan (CS), can not only improve the control of drug release but also changes the surface charge from negative to positive, thereby increasing the concealing properties of these NPs from the immune system, and extending the shelf life of the drug [19,20].

Nanocarriers are able to deliver drugs to target cells through inactive and active mechanisms. In cancer therapy, the presence of blood vessel abnormalities allows nanome-



ter carriers to enter the tumor growth environment; the dysfunction of the lymphatic system causes insufficient drainage and allows the drug to accumulate in the tumor growth microenvironment. This increases the effectiveness of the treatment owing to the effect of enhanced permeation and retention (EPR) [18,21]. Active drug delivery is possible through the interaction between ligands that are attached to nanocarriers and receptors on the surface of target cells (with high expression) [22,23]. Using the EPR effect, this approach increases drug internalization through receptor-mediated uptake and increases drug delivery to cancer cells [24,25]. High expression of folic acid (FA) receptors on the surface of malignant cells, compared to normal cells, has made this ligand a suitable candidate for surface modification of NPs and the specific targeting of cancer cells. The high tendency of this ligand to bind to nanocarriers, its non-toxicity, and its non-immunogenicity are other advantages of FA, compared to other ligands [22].

The current study aimed to develop an optimal and targeted formulation for the transfer of AC to breast cancer cells. Thus, SLN was used for loading, and then, NP surfaces were decorated with CS attached to FA. After studying the physicochemical properties, the antioxidant effects and toxicity of AC-SLN-CS-FA on cancer cells were evaluated, and the inhibition mechanism of the NPs was investigated based on the apoptosis process.

## 2. Materials and Methods

### 2.1 Materials

Human foreskin fibroblast (HFF) and MCF-7 breast cancer cell lines were purchased from the cell bank at the Research Institute of Biotechnology, Ferdowsi University of Mashhad, Mashhad, Iran. To ensure the authenticity of the cells, DNA profiling of short tandem repeats (STRs) was utilized and regular screening for mycoplasma contamination was conducted. Stearic acid, CS (LMW), non-ionic surfactant (Tween 80), lecithin, N-hydroxysuccinimide (NHS), ethanol (EtOH), 1-Ethyl-3-(3-dimethylaminopropyl)carbodiimide (EDC), potassium persulfate (PPS), dimethylsulfoxide (DMSO), 2,2-Diphenyl-1-picrylhydrazyl (DPPH), and 2,2'-azino-bis(3-ethylbenzothiazoline-6-sulfonic acid) (ABTS) were obtained from Merck (Darmstadt, Germany). AC, propidium iodide (PI), acridine orange (AO), phosphate-buffered saline (PBS), and 2,5-diphenyl-2H-tetrazolium bromide (MTT) were purchased from Sigma-Aldrich (St. Louis, MO, USA). FBS was bought from Gibco (Franklin Lakes, NJ, USA). Cell culture medium, antibiotics, and trypsin EDTA were obtained from Invitrogen (Carlsbad, CA, USA).

### 2.2 Synthesis of AC-SLN

SLN, in which the AC was passively loaded, was prepared using homogenization and ultrasonication. Stearic acid was used as a lipid component, and Tween 80 and

lecithin were used as surfactants and co-surfactants. To prepare the lipid phase, 10 mg of AC, dispersed in distilled water, was added to the mixture containing stearic acid and lecithin, and the temperature of the mixture was raised to 85 °C. The aqueous phase was prepared by mixing water and Tween 80. After the isothermalization of lipid and aqueous phases (at 85 °C), the aqueous phase was added to the lipid phase, and the mixture was homogenized using a high-pressure homogenizer (HPH) at 85 °C for 5 minutes. After 24 h of storage at room temperature, the final mixture was centrifuged using a high-speed centrifuge and the collected supernatant was used for HPLC analysis and to evaluate the amount of free AC. The HPLC system (Alliance 2695, Waters, Milford, MA, USA) was equipped with a UV detector and consisted of C18 as a stationary phase. The column was operated in isocratic mode (50:50 MeOH: H<sub>2</sub>O) at a flow rate of 0.5 mL/min. The UV detector was set at 254 nm for the measurement of AC.

### 2.3 Surface Modification of AC-SLNs with CS-FA

To modify the surface of AC-SLN, a CS coating attached to FA was used. For this purpose, CS attached to FA was first prepared, and then, added to the mixture containing the NPs. To prepare CS-FA, FA powder was dissolved in DMSO, and EDC and NHS were added to it. After incubating for 1 h, the resulting mixture was filtered. To connect CS to FA, CS powder was dissolved in 1% acetic acid, and after ensuring its dissolution, the resulting mixture was added to the FA-NHS mixture and incubated for 24 h on a magnetic stirrer. Next, by adjusting the pH to 9, a CS precipitate of FA was formed, which was dialyzed, and then, lyophilized to remove free FA. To decorate the NP surfaces, CS-FA powder was dissolved in 1% acetic acid and added to SLNs dissolved in distilled water (DW). The final mixture was mixed for 2 h under continuous stirring and after centrifugation, was lyophilized. The supernatant was used for HPLC analysis and to determine the percentage of FA binding to the surface of the NPs.

### 2.4 AC-SLN-CS-FA Characterization

Average size and surface charge along with the dispersion distribution of AC-SLN-CS-FA were evaluated by DLS. Firstly, a suspension containing AC-SLN-CS-FA dissolved in DW (1:100) was prepared. Then, after ensuring that the NPs were dispersed, the resulting suspension was analyzed under a scattering angle of 170 degrees at a temperature of 25 °C. FESEM was used to examine the morphology of the samples. For this purpose, NPs were dispersed in DW and sonicated. Next, a drop of the resulting solution was sprinkled on aluminum foil and left to dry. After the solvent had dried, the surface of the sample was coated with gold and subjected to microscopic examination. The samples for FTIR were prepared by compressing NPs with potassium bromide (KBr) into pellets, which were analyzed in the FTIR device.

### 2.5 Assessment of FA Binding and AC Entrapment Efficiency

Spectrophotometer absorption was used to evaluate the AC encapsulation and FA binding percentages. For this purpose, the amount of free substance was measured and subtracted from the total substance. The remainder was entered into the reaction and the amount of trapped substance was observed. This method is called the indirect method. A serial concentration of AC was prepared, and then, the absorption of each sample was measured and the related standard graph was drawn. Next, the absorbance of the supernatant (Section 2.2) was measured at the same wavelength. By inserting it into the formula obtained from the standard curve, the amount of free AC in the supernatant was obtained, and finally, the percentage of encapsulation efficiency (EE%) of the substance was calculated using the formula below:

$$EE (\%) = (\text{total amount of drug} - \text{the amount of free drug}) / \text{total amount of drug} \times (100).$$

The same method was used to evaluate the level of FA binding. Standard curves related to different FA concentrations were drawn, and the amount of FA binding was obtained by placing the amount of absorption obtained from the supernatant in Section 2.3 and replacing the numbers in the above formula.

### 2.6 AC Release

Dialysis method and absorption spectrophotometry were used to evaluate drug release within 5 days. Firstly, the free AC and NPs were dispersed in the phosphate buffer and poured into the dialysis bag, which had already been activated. The lid of the bag was closed, and the bag was suspended in the phosphate buffer at 37 °C and 100 rpm. At certain time intervals, 1 mL of the phosphate buffer was removed from around the bag to check the amount of released substance, and 1 mL of fresh buffer was re-added to the beaker. Then, the collected samples were analyzed by spectrophotometry. The drug release graphs were drawn in Microsoft Excel.

### 2.7 ABTS and DPPH Scavenging Activity of AC-CFS-NPs

Firstly, ABTS and DPPH free radicals were prepared. To prepare the ABTS free radicals, a solution containing distilled water, PPS, and ABTS was prepared and incubated in the dark for 24 hours. Then, the solution was diluted with DW until it reached an absorbance of 0.7 at a wavelength of 734 nm. DPPH free radicals were prepared using 96% EtOH, in which DPPH powder was dissolved. Next, different concentrations of NPs were prepared and equal volumes of the desired free radical were added. Then, the samples containing ABTS free radicals were incubated for one hour in the dark at room temperature, after which, their absorbance was recorded at a wavelength of 734 nm. The samples containing DPPH free radicals were incubated for 30 minutes in the incubator and analyzed at a wavelength of 517 nm.

### 2.8 Cytotoxic Assay

To conduct the cytotoxic assay, cells were seeded in 96-well plates for 24 h, after which, they were treated with different doses of AC-SLN-CS-FA for 48 h. Next, the medium containing AC-SLN-CS-FA was drained from each well, and 20 µL of MTT solution was added. After 4 h, the required time for the reaction to be completed, the plates containing the cells were removed from the incubator, and the MTT medium was drained. The formazan crystals, formed by the MTT reaction with living cells, were dissolved by adding DMSO (100 µL) to each well. Then, the absorbance of the samples was measured at a wavelength of 570 nm. By replacing the numbers in the formula below, the cell viability following the treatment with the NPs was calculated and compared to the untreated cells.

$$\text{Viability of cells (\%)} = \text{OD}_{\text{sample}} / \text{OD}_{\text{control}} \times (100).$$

### 2.9 AO/PI Double Staining Assay

For staining, cells were first cultured in 6-well plates, and then, treated with different concentrations of AC-CFS-NPs. After the treatment period, the treatment medium was drained and 1 mL of PBS containing AO (1 µL; 1 mg/mL) and PI (1 µL; 1 mg/mL) dye was added to each well. Finally, images of the cells were taken using a fluorescent inverted microscope.

### 2.10 Flow Cytometry

Firstly, the cells were transferred to a 6-well plate. After incubating for 24 h, the cells were subjected to different concentrations of AC-SLN-CS-FA for 48 h. Afterward, the medium containing the treatment was drained, the cells were washed with PBS, and trypsin was added to each well. After ensuring that the cells were separated, the cell suspension was transferred to separate microtubes and centrifuged. After the supernatant was removed, 300 microliters of PI dye were added to the cell sediment and analyzed by flow cytometry (Becton Dickinson, Maryland, MD, USA) after 15 min of incubation.

### 2.11 Real-Time qPCR Analysis

The effects of AC-SLN-CS-FA treatment on expression levels of apoptotic genes *BAX*, *Bcl-2*, and *caspase-8* were evaluated. Table 1 shows the primer list. Cells were treated ( $1 \times 10^6$ ) with various doses of AC-SLN-CS-FA for 48 h. Next, the cells were separated from the bottom of the flask, and the total RNA was isolated using the Biotech kit. The amount of RNA was assessed by the nanodrop method, and then, cDNA was synthesized using the RNA strand. The reaction mixture was prepared to contain cDNA with water, SYBR green, and special primers, in a volume of 20 microliters, and analyzed using the following temperature-time conditions in the Bio-Rad device: the holding step included 95 °C, 15 min for 1 cycle; the annealing step included 95 °C, 15 s, 58.5 °C, 20 s, and 39 cycles; the extension step included 72 °C, 20 s, and 39 cycles; and the melt-

**Table 1. List of primers used for real-time PCR.**

Gene	Forward	Reverse	Amplicon length (bp)	Genebank No.
<i>GAPDH</i>	TGCTGGTGCTGAGTATGTCG	GCATGTCAGATCCACAACGG	131	NM_002046
<i>Caspase-8</i>	GAAAAGCAAACCTCGGGGATAC	CCAAGTGTGTTCCATTCTGTC	113	NM_033355.4
<i>BAX</i>	TTTGCTTCAGGGTTTCATCCA	CTCCATGTTACTGTCCAGTTCGT	151	NM_138764.5
<i>Bcl-2</i>	CATGTGTGTGGAGAGCGTCAAC	CAGATAGGCACCCAGGGTGAT	241	NM_000633.3

ing step included 65–95 °C for 1 cycle. The delta–delta Ct ( $\Delta\Delta C_t$ ) method was used to evaluate the relative changes in gene expression. GAPDH was used as a reference gene.

### 2.12 Statistical Analysis

Data were analyzed by one-way ANOVA using the GraphPad Prism software (version 8) (GraphPad Software, Inc., San Diego, CA, USA). Variance was analyzed and means were compared using the LSD method. A significance level of  $p < 0.05$  was used to determine the statistical significance of the results.

## 3. Results

### 3.1 Characterization of AC-SLN-CS-FA

Fig. 1A and B show acceptable physicochemical properties for AC-SLN-CS-FA. As indicated, NPs had a Z-average of  $245.7 \pm 10.7$  nm with an average diameter of  $86.7 \pm 9.4$  nm, reported by number. The NPs had a uniform size distribution with a PDI of 0.31. The small size of the particles along with the dispersion index of less than 0.5 indicated their stability and lower tendency to accumulate [26,27]. The zeta potential of the NPs was  $+21.3 \pm 7.9$  mV. The surface charge of the nanoparticles can also provide information on the stability of particles, considering that a higher surface charge of  $\pm 20$  mV in lipid NPs was sufficient to prevent the agglomeration of the particles [28,29]. Thus, it can be said that the synthesized NPs have ideal stability. In addition to the size, distribution, and surface charge of the NPs, their morphology also affected some of their characteristics, such as EE%, ligand-receptor binding ability, and cellular absorption [30,31]. Microscopic images (Fig. 1C) show spherical NPs with smooth surfaces. The prepared images also show NPs with dimensions below 100 nm, which are comparable to the DLS results. In Fig. 1D, the characteristic peaks of SLN-NPs are shown as strong peaks at 2862.7, 2919.6, and 1466  $\text{cm}^{-1}$ , corresponding to O-H, C-H, and C=C bonds, respectively [32]. The peak present at 1723  $\text{cm}^{-1}$  is related to C=O bonds, which indicates the formation of CS-FA and confirms the successful surface modification of NPs with CS.

### 3.2 FA Binding and AC Entrapment Efficiency

According to the formula obtained from the standard curve for AC ( $y = 0.3631x + 0.0763$ ,  $R^2: 0.99$ ) and FA ( $y = 0.8361x + 0.2414$ ,  $R^2: 0.97$ ), and by replacing the absorption of the supernatant in these formulations, the amounts of AC and free FA were calculated. Next, the EE of AC

was reported to be 86.3%, and the amount of bound FA was 63%.

### 3.3 AC Release

Fig. 2 shows the drug release profile. The release of free AC from the dialysis tubing reached 100% during the first 24 h of the study. The result exhibited 70.5% cumulative drug release after 5 days. This graph shows more drug release during the first 24 h because of the release of drug molecules located on the surface of the NPs [22]. The slow release of the drug after the initial burst release indicates the entrapment of the drug throughout the nanocarrier and the effectiveness of the formulation in the continuous and controlled release of the drug.

### 3.4 Free Radical Scavenging Capacity of AC-SLN-CS-FA

Investigation of ABTS and DPPH free radicals inhibition rates in the presence of AC-SLN-CS-FA by spectrophotometer absorption method at 734 and 517 nm wavelengths revealed the high inhibitory effects of AC-SLN-CS-FA on DPPH free radicals. As shown in the graph (Fig. 3), NPs are capable of inhibiting both free radicals in a concentration-dependent manner. Increasing the concentration of the NPs to about 250  $\mu\text{g}/\text{mL}$  caused more than an 80% inhibition of both free radicals; however, in low concentrations, a greater inhibition of DPPH free radicals was observed. These results show the antioxidant power of NPs in inhibiting free radicals and preventing damage by oxidative stress.

### 3.5 Cytotoxic Capacity of AC-SLN-CS-FA

Since the MTT reaction utilizes the succinate dehydrogenase enzyme of living cells and the production of purple formazan crystals, it was used to evaluate the percentage of cell viability in the presence of AC-SLN-CS-FA. The cytotoxicity effects of free AC were evaluated against normal HFF and MCF-7 cancer cells, and no toxicity was observed in the free AC data compared to the HFF cells. However, significant cytotoxicity was observed in the effects of free AC against MCF-7 cells ( $p < 0.01$  and  $p < 0.001$ , respectively). The results shown in Fig. 4A–D reveal the higher inhibitory effect that AC-SLN-CS-FA had against MCF-7 cells compared to normal cells. Additionally, AC-SLN-CS-FA exhibited no detectable toxicity effect on HFF cells at any of the investigated concentrations, whereas, AC-SLN-CS-FA had an inhibitory  $\text{IC}_{50}$  of  $\sim 20$   $\mu\text{g}/\text{mL}$  in the MCF-7 cells. These results show the selective toxicity of AC-SLN-CS-FA on malignant cells and its safe application on normal cells.

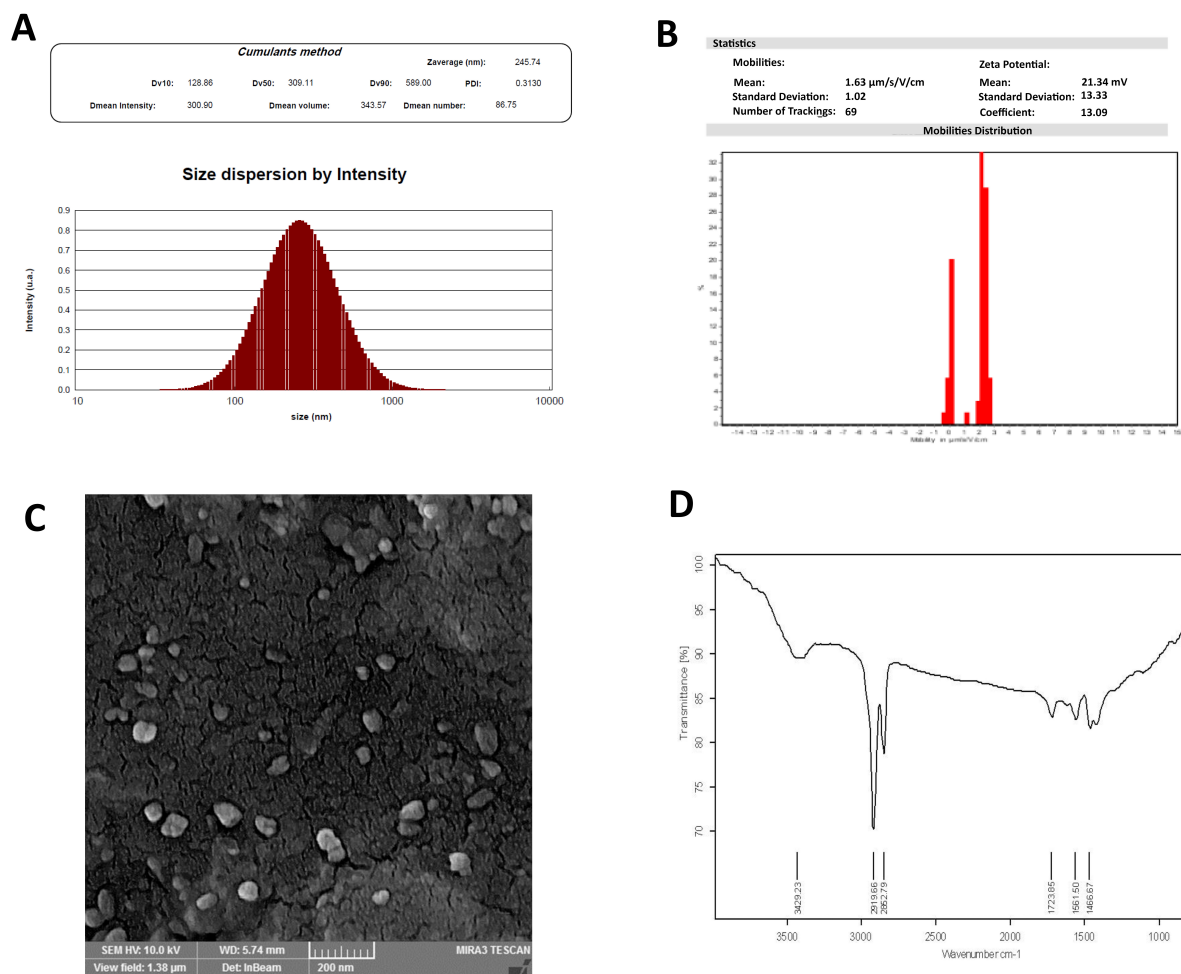


**Fig. 1. Characterization of AC-SLN-CS-FA.** (A) Results for size. (B) Results for zeta-potential of AC-SLN-CS-FA. (C) FESEM image of AC-SLN-CS-FA; and (D) FTIR spectrum of AC-SLN-CS-FA. PDI, polydispersity index.

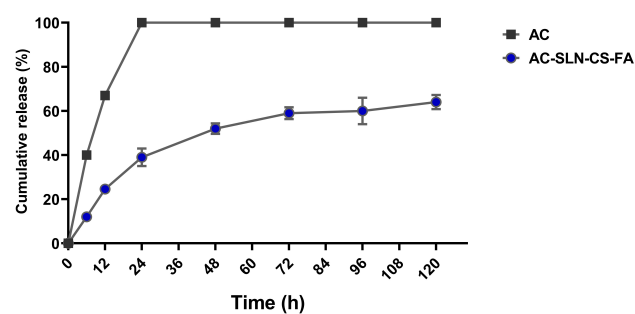


**Fig. 2. Release Study.** Release of free AC from dialysis tubing and AC from AC-SLN-CS-FA. Data were presented as mean  $\pm$  SD.

### 3.6 Fluorescence Staining Assay

Fluorescent dyes were used to examine the cell morphologies and their changes during treatment. AO dye can penetrate living cells, and after penetration, it causes a green color to be emitted, while PI penetrates damaged cells and causes a red color to be emitted. Fig. 4 shows the mor-

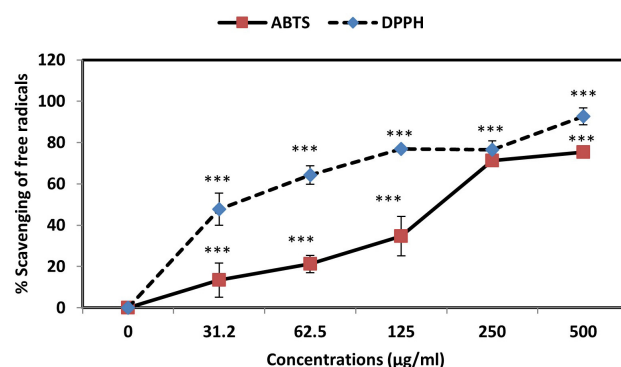


**Fig. 3. Percentage inhibition of ABTS and DPPH free radicals in the presence of AC-SLN-CS-FA.** Data were presented as mean  $\pm$  SD. (n = 3, \*\*\*  $p < 0.001$ ). DPPH, 2,2-diphenyl-1-picrylhydrazyl; ABTS2, 2'-azino-bis(3-ethylbenzothiazoline-6-sulfonic acid).

phological images of the stained cells. As can be seen, all the cells in the untreated group are green and have a normal morphology; in the treated groups, however, the num-

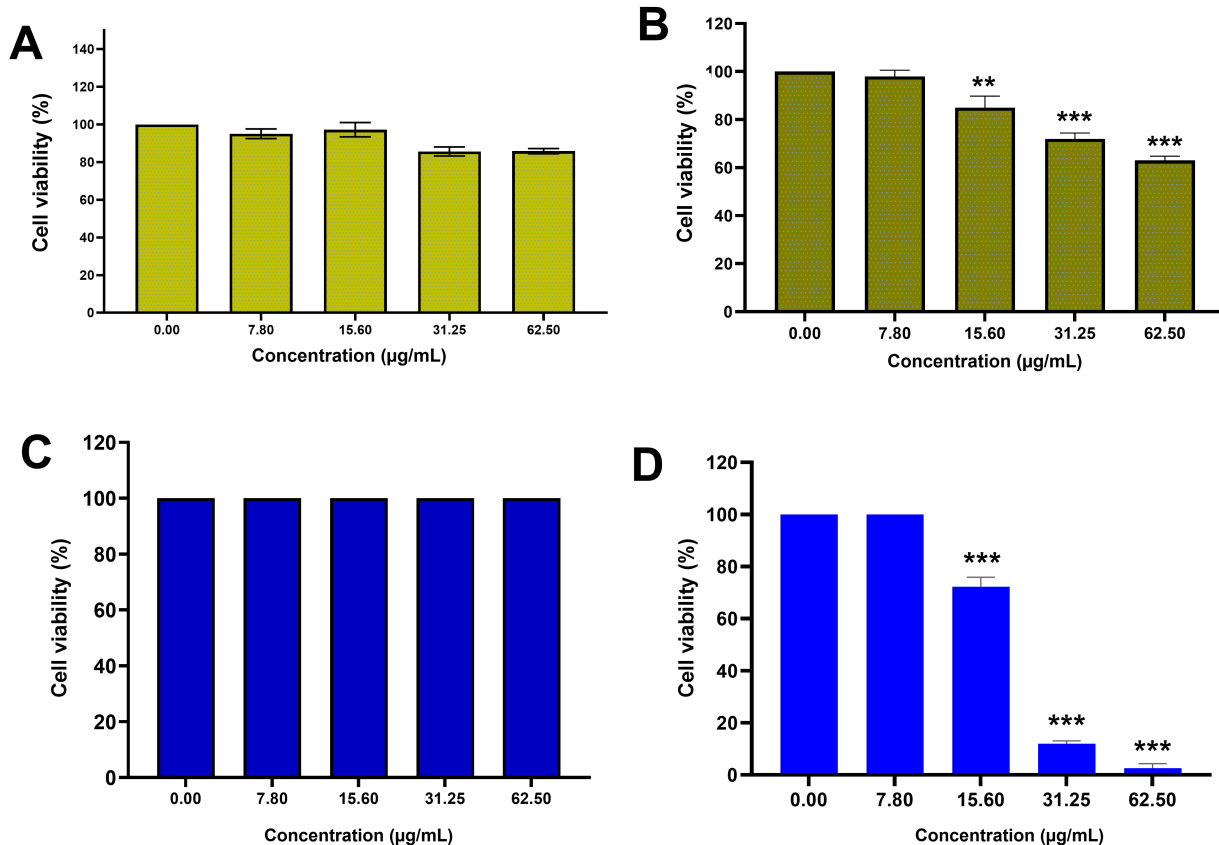


**Fig. 4. Cytotoxicity study.** MTT results: (A) Cytotoxicity effects of AC against HFF cells; (B) cytotoxicity effects of AC against MCF-7 cells; (C) cytotoxicity effects of AC-SLN-CS-FA against HFF cells; (D) cytotoxicity effects of AC-SLB-CS-FA against MCF-7 cells. Data were presented as mean  $\pm$  SD. (n = 3, \*\*  $p < 0.01$  and \*\*\*  $p < 0.001$ ).

ber of cells emitting an orange color gradually increases as the treatment concentration increases, thereby indicating an increase in the presence of apoptotic cells. Furthermore, the morphological change of the cells to a spherical state is a characteristic of apoptotic cells, and can be observed in Fig. 5. The staining results exhibit that apoptosis increases in accordance with the increasing treatment concentrations.

### 3.7 Flow Cytometry Results

Fig. 6 shows that 4.15%, 65%, 9.17%, and 15.8% of the cells in the control group are in the sub-G1, G1, S, and G2–M phases, respectively. However, in the AC-SLN-CS-FA-treated cells, a decrease is observed in the percentage of cells in all phases of the cell cycle, except the sub-G1 phase, which shows the effect of AC-SLN-CS-FA on increasing the percentage of cells in this phase. Since sub-G1 phase cells are known to be apoptotic cells, these findings show the effect of AC-SLN-CS-FA on the induction of apoptosis in treated cells. No arrest was observed in any cell cycle stages other than sub-G1 in the treated cells.

### 3.8 Analysis of Apoptosis-Related Genes

The results of the RNA analysis showed a change in *BAX* and *Bcl-2* gene expressions, leading to the activation

of the internal apoptotic pathway. Upregulation of the *BAX* gene and downregulation of *Bcl-2* represents the activation and suppression of pro- and antiapoptotic genes, respectively, thereby indicating the induction of apoptosis in the treated cells. The extrinsic apoptotic pathway was investigated by analyzing *caspase 8* gene expression levels. The *caspase 8* expression levels showed no significant change compared to the control, which indicates the inactivity of the external pathway and the occurrence of apoptosis from the internal pathway (Fig. 7).

## 4. Discussion

The use of drug delivery systems based on lipids, proteins, polymers, etc., decorated with different ligands for passive and active targeting, has made it possible to further internalize drugs to target cells, while increasing the solubility, stability, and bioavailability of the drug and reducing the treatment side effects [33].

In this study, SLNs were used to encapsulate AC, a hydrophobic compound with pharmacological properties whose therapeutic effects on a wide range of diseases, including inflammatory diseases, diabetes, cancer, and degenerative diseases, have been reported in various studies. The loading of this compound into SLNs, while in-

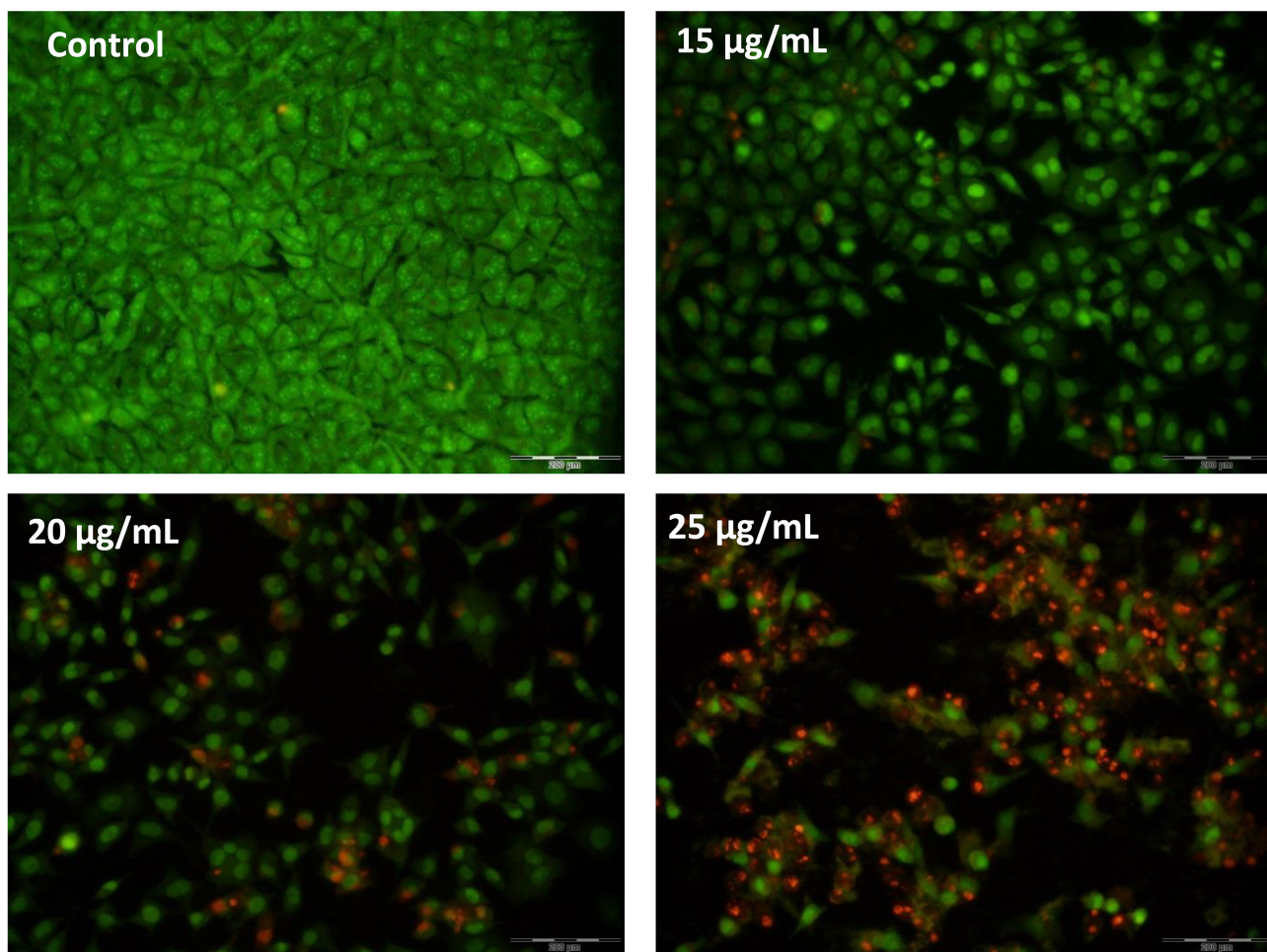


**Fig. 5. AO/PI double-staining.** The increase in red-color-emitting cells during the increase in treatment concentrations indicates the proapoptotic effects of AC-SLN-CS-FA on MCF-7 cells.

creasing its stability, prevents it from being trapped by proteins and fatty acids in cell membranes and facilitates its improved delivery to target cells. In the prepared formulation, stearic acid was used as a physiological lipid with no toxicity and the possibility of encapsulating hydrophobic compounds with high efficiency. Part of the stability of this formulation can be attributed to the presence of the Tween 80 surfactant and the lecithin co-surfactant since the type of surfactant and its amount in the formulation significantly impact the stability, physicochemical properties, and biological properties of the NPs. In addition to the type and concentration of formulation components, the preparation techniques and temperatures also affect the quality and physicochemical properties of the NPs, including drug loading and particle size [34–36]. In this study, similar to other studies, the hot homogenization and probe-sonication technique was used to prepare the formulation [18,37]. In addition to this method, other studies have used methods such as solvent evaporation [16], homogenization, and ultrasound [18,37] to prepare different formulations with different properties.

In preparing SLNs, part of the drug is loaded on the surface or intermediate phase of the NPs, which causes the explosive release of the drug under systemic conditions and is known as a limitation for the use of SLNs. Conversely, SLNs have a hydrophobic nature and a negative surface charge. These properties provide the possibility for them to be detected by the RES and cause their rapid removal by opsonin proteins [38]. NP surface modification can play an important role in overcoming these limitations. Coating NPs with cationic polymers, such as CS, while changing the charge of the nanoparticles from negative to positive, can control the release of the drug under systemic conditions and increase the stability and effectiveness of the drug. Mucosal adhesion and increased CS permeability [39] make it a suitable adjuvant in nanoformulations. CS mucosal adhesion is associated with a positive surface charge of the macromolecule, which in turn is affected by the protonation of the amino group at different pHs [40]. Therefore, in CS-based systems, due to pH sensitivity, they provide the possibility of purposefully delivering the drug to any area of the body [41]. In the current study, CS coating was

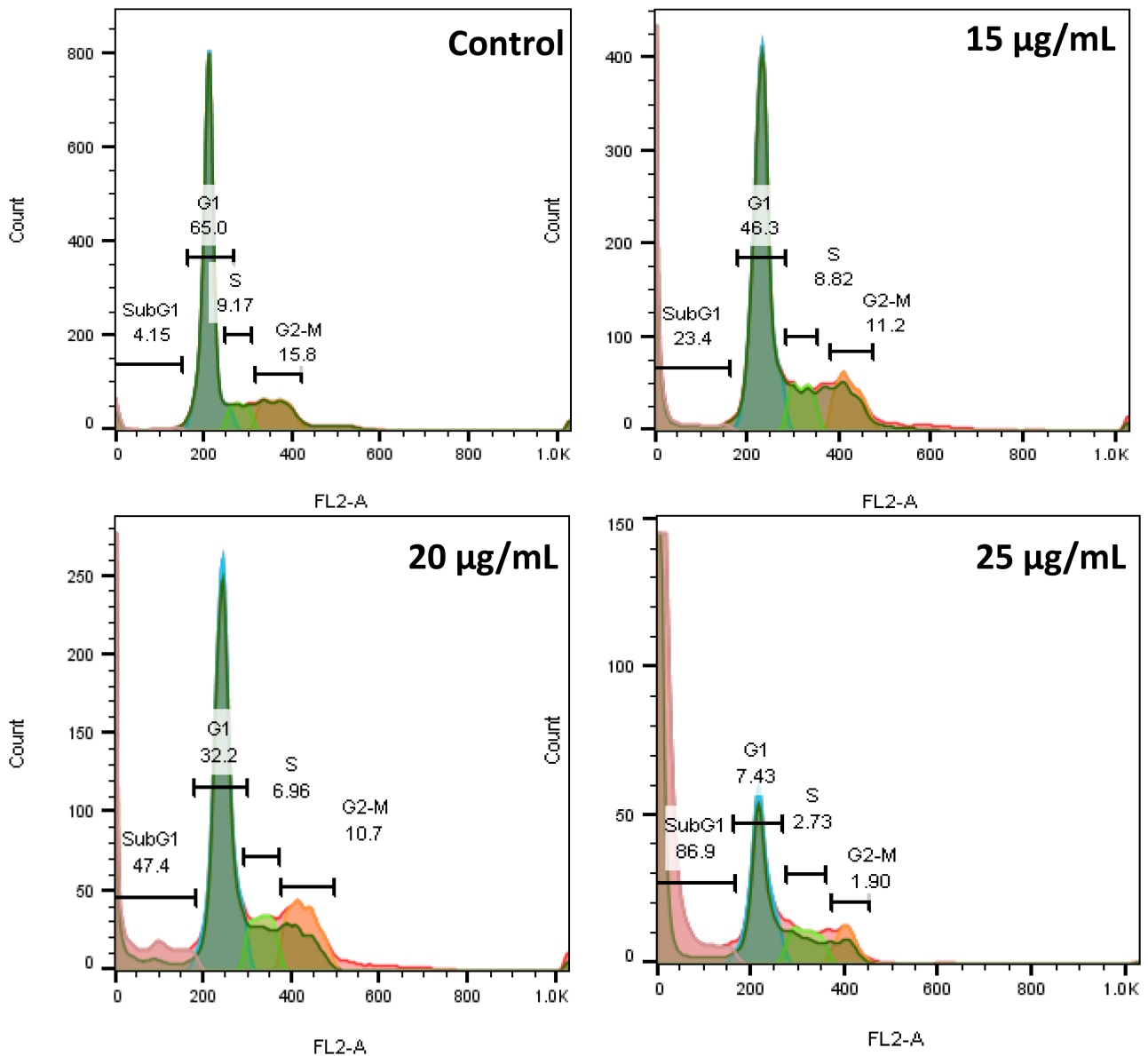


**Fig. 6.** The flow cytometry diagram shows the cells arresting in the sub-G1 phase after treatment with AC-CFS-NPs.

used for targeted drug delivery, and FA ligand binding was also used at the NP surface. The physicochemical properties (Fig. 1) of the NPs showed colloidal dispersions with an average diameter of 86 nm, acceptable stability (+21.34 mV), and uniform distribution (PDI: 0.31). In a 2017 study, CS-coated SLNs containing cinnamon/oregano with a size of 254.77 nm, a surface charge of 15.26 mV, and a dispersion index of 0.28 were synthesized, which is comparable to the physicochemical properties used in the present study [19]. In another study, SLNs decorated with CS-FA were used to transfer trans-resveratrol-ferulic acid to colon cancer cells [22]. These NPs, similar to the present study, had nanometer dimensions (174 nm) with uniform dispersion (0.16), while the surface charge of the nanoparticles was reported despite the CS +25 mV coating [22].

The encapsulation efficiency of the drug in SLNs is

related to the crystalline state of the formulation and the composition of its lipid matrix. In the present study, this index was reported to be 83% for AC, which is comparable to previous studies [42–44]. Successful encapsulation of AC in SLNs can be related to the hydrophobic nature of AC and its high binding energy to the lipid matrix of SLNs [45]. The most valuable indicators of a drug delivery system are the drug loading percentage and the controlled release in the body. The amount of drug loading depends on various factors, including the materials used in the formulation, the type of drug, and its nature [26]. The present study has reported the drug release index as burst propagation followed by slow release (Fig. 2). This burst release can be attributed to the presence of unencapsulated drug molecules at the SLN level or in the peripheral dispersion of the formulation [22]. The prolonged release of the AC from

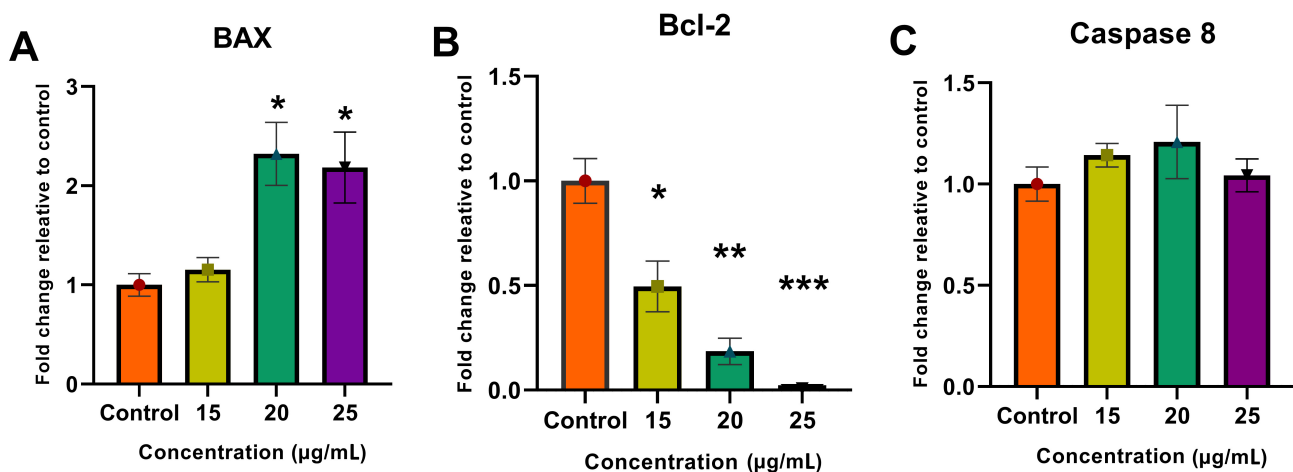


**Fig. 7. Real-time qPCR analysis.** Molecular analysis showed an increase in (A) *BAX* gene expression and a decrease in (B) *Bcl-2* expression along with no change in (C) *caspase 8* expression using the delta-delta Ct ( $\Delta\Delta Ct$ ) method (mean  $\pm$  SD,  $n = 3$ , \*  $p < 0.05$ , \*\*  $p < 0.01$ , and \*\*\*  $p < 0.001$ ; 0, 15, 20, and 25 are the concentrations of AC-SLN-CS-FA in  $\mu\text{g/mL}$ ).

AC-SLN-CS-FA compared to free AC indicated the entrapment of AC in all parts of the formulation. The AC release index generally showed a slow and long-term release, and this pattern can reduce the need for high doses of drug by maintaining the drug concentration for a long time [46].

In this study, the anticancer effects of the nanoparticles were evaluated based on different cellular and molecular mechanisms. The antioxidant power of NPs plays an effective role in preventing malignancy and its progression in the body. Examination of the ability of AC-SLN-CS-FA to inhibit ABTS (165.72  $\mu\text{g/mL}$ ) and DPPH (36.05  $\mu\text{g/mL}$ ) free radicals revealed the anticancer effects of this compound in preventing the accumulation of free radicals and the damage caused by them. The antioxidant power and role of AC in inhibiting free radicals have been reported in previous literature. The results of these studies report the role of AC in reducing oxidative stress and its damage. In addition, inhibition of superoxide, hydroxyl, and nitric oxide (NO) free radicals by AC has been reported [47]. It is essential to control redox status in order to preserve cancer cells after treatment [48]. As a result of the high basal levels of reactive oxygen species (ROS), cancer cells are more susceptible than normal cells to additional ROS increases. However, by upregulating their antioxidant systems, chemoresistant cancer cells become highly adapted to intrinsic oxidative stress or drug-induced oxidative stress [49]. Decomposition of AC occurs rapidly, resulting in hydrogen sulfide being produced in the process. In the regulation of blood pressure, hydrogen sulfide acts as a gaseous signaling molecule. It also regulates smooth muscle relaxation, dilation of arteries, and lowering of blood pressure. The downregulation of angiotensin II type 1 receptor and the NF-E2-related factor-2 (NRF2)-inhibitor Keap1 have been shown to facilitate the antioxidant of AC [47,50].

The safety of NPs on normal cells and their ability to

remove malignant cells is one of the most important features that are examined in any formulation. The results of this study showed the toxicity of NPs against breast cancer cells with an average concentration of 21  $\mu\text{g/mL}$ , while no toxicity effect was observed on normal cells. The high inhibitory effect of NPs against cancer cells can be attributed to the presence of CS and FA ligands on the surface of NPs. Various studies have reported similar results in this area [18,51,52].

One of the most important reasons for the malignancy of cells is their proliferation and escape from apoptosis [53], meaning the identification of molecules capable of inducing apoptosis can play an effective role in inhibiting cancer cells. In this study, the role of AC-SLN-CS-FA in activating the intrinsic pathway of apoptosis in breast cancer cells was reported through increased *BAX* expression and decreased *BCL-2* expression. The lack of any significant change in the expression of *caspase 8*, which is involved in the activation of the extrinsic apoptotic pathway, may confirm the above results (Fig. 7). In previous literature, the role of AC in activating the intrinsic pathway by increasing the expression of caspases 3 and 9 has been reported [54]. The current study reported a decreasing effect of AC on STAT3 followed by decreased cell proliferation, angiogenesis, and induction of apoptosis in treated cells [54]. Another study has reported proapoptotic effects of AC on liver cancer cells through increases in the percentage of sub-G1 phase cells as well as nucleation changes during DAPI staining [55]. In the present study, the role of AC-SLN-CS-FA on cell cycle arrest in the sub-G1 phase in MCF-7 cancer cells (Fig. 6) was confirmed, while the morphological cell changes observed during fluorescent staining (Fig. 5) confirmed the occurrence of apoptosis in cells treated with AC-SCF-NPs. Activation of apoptosis signaling and inhibition of cell proliferation resulting from the treatment of

cells with SLNs loaded with various bioactive compounds have been reported in many previous studies [56,57], which are comparable to the present study. Differences in the activation of different mechanisms that inhibit cancer cells can be attributed to differences in the physicochemical properties of the formulation and the effects of the loaded drug.

## 5. Conclusions

The results of the present study show the formation of monodispersed (0.3), stable NPs (+21.34 mV) with nanometer dimensions (86.75 nm). The efficacy of the prepared formulation is shown by the 86.3% AC loading and 63% FA binding along with a long-release profile. The ability of AC-SLN-CS-FA to inhibit free radicals and its inhibitory effect on cancer cells through the activation of the intrinsic apoptosis pathway introduces this NP as an appropriate candidate for preclinical cancer investigations.

## Availability of Data and Materials

The data that support the findings of this study are available upon reasonable request from the authors.

## Author Contributions

FJA: Validation, Formal analysis, Investigation, Data curation, Methodology, Formal analysis, and Writing – original draft. MG: Supervision, Validation, Data curation and Writing – review & editing. MHT: Supervision, Validation, Data curation, Methodology, and Writing – review & editing. All authors read and approved the final manuscript. All authors have participated sufficiently in the work and agreed to be accountable for all aspects of the work.

## Ethics Approval and Consent to Participate

Not applicable.

## Acknowledgment

Not applicable.

## Funding

This research received no external funding.

## Conflict of Interest

The authors declare no conflict of interest.

## References

- [1] Güney G, Kutlu HM. Importance of solid lipid nanoparticles in cancer therapy. *Nanotechnology*. 2011; 3: 400–403.
- [2] Bayón-Cordero L, Alkorta I, Arana L. Application of Solid Lipid Nanoparticles to Improve the Efficiency of Anticancer Drugs. *Nanomaterials (Basel, Switzerland)*. 2019; 9: 474.
- [3] Chen X, Li H, Xu W, Huang K, Zhai B, He X. Self-Assembling Cyclodextrin-Based Nanoparticles Enhance the Cellular Delivery of Hydrophobic Allicin. *Journal of Agricultural and Food Chemistry*. 2020; 68: 11144–11150.
- [4] Kamelan Kafi M, Bolvari NE, Mohammad Pour S, Moghadam SK, Shafaei N, Karimi E, *et al.* Encapsulated phenolic compounds from *Ferula gummosa* leaf: A potential phyto-biotic against *Campylobacter jejuni* infection. *Journal of Food Processing and Preservation*. 2022; 46: e16802.
- [5] Sarvizadeh M, Hasanpour O, Naderi Ghale-Noie Z, Mollazadeh S, Rezaei M, Pourghadamyari H, *et al.* Allicin and Digestive System Cancers: From Chemical Structure to Its Therapeutic Opportunities. *Frontiers in Oncology*. 2021; 11: 650256.
- [6] Karimi M, Gheybi F, Zamani P, Mashreghi M, Golmohammadzadeh S, Darban SA, *et al.* Preparation and characterization of stable nanoliposomal formulations of curcumin with high loading efficacy: *In vitro* and *in vivo* anti-tumor study. *International Journal of Pharmaceutics*. 2020; 580: 119211.
- [7] Zarei M, Karimi E, Oskoueian E, Es-Haghi A, Yazdi MET. Comparative Study on the Biological Effects of Sodium Citrate-Based and Apigenin-Based Synthesized Silver Nanoparticles. *Nutrition and Cancer*. 2021; 73: 1511–1519.
- [8] Beyrami M, Karimi E, Oskoueian E. Synthesized chrysin-loaded nanoliposomes improves cadmium-induced toxicity in mice. *Environmental Science and Pollution Research International*. 2020; 27: 40643–40651.
- [9] Kaur R, Sharma N, Tikoo K, Sinha VR. Development of mirtazapine loaded solid lipid nanoparticles for topical delivery: Optimization, characterization and cytotoxicity evaluation. *International Journal of Pharmaceutics*. 2020; 586: 119439.
- [10] Mohammed HA, Khan RA, Singh V, Yusuf M, Akhtar N, Sulaiman GM, *et al.* Solid lipid nanoparticles for targeted natural and synthetic drugs delivery in high-incidence cancers, and other diseases: Roles of preparation methods, lipid composition, transitional stability, and release profiles in nanocarriers' development. *Nanotechnology Reviews*. 2023; 12: 20220517.
- [11] Tabatabaeain SF, Karimi E, Hashemi M. *Satureja khuzistanica* Essential Oil-Loaded Solid Lipid Nanoparticles Modified With Chitosan-Folate: Evaluation of Encapsulation Efficiency, Cytotoxic and Pro-apoptotic Properties. *Frontiers in Chemistry*. 2022; 10: 904973.
- [12] Madkhali OA. Perspectives and Prospective on Solid Lipid Nanoparticles as Drug Delivery Systems. *Molecules (Basel, Switzerland)*. 2022; 27: 1543.
- [13] Arduino I, Liu Z, Rahikkala A, Figueiredo P, Correia A, Cutrignelli A, *et al.* Preparation of cetyl palmitate-based PEGylated solid lipid nanoparticles by microfluidic technique. *Acta Biomaterialia*. 2021; 121: 566–578.
- [14] Albekery M, Alharbi K, Alarifi S, Ahmad D, Omer M, Massadeh S, *et al.* Optimization of a nanostructured lipid carriers system for enhancing the biopharmaceutical properties of valsartan. *Digest journal of Nanomaterials and Biostructures*. 2017; 12: 381–389.
- [15] Basha SK, Dhandayuthabani R, Muzammil MS, Kumari VS. Solid lipid nanoparticles for oral drug delivery. *Materials Today: Proceedings*. 2021; 36: 313–324.
- [16] Khan AS, Shah KU, Mohaini MA, Alsalman AJ, Hawaj MAA, Alhashem YN, *et al.* Tacrolimus-Loaded Solid Lipid Nanoparticle Gel: Formulation Development and *In Vitro* Assessment for Topical Applications. *Gels (Basel, Switzerland)*. 2022; 8: 129.
- [17] Mashreghi M, Faal Maleki M, Karimi M, Kalalinia F, Badiie A, Jaafari MR. Improving anti-tumour efficacy of PEGylated liposomal doxorubicin by dual targeting of tumour cells and tumour endothelial cells using anti-p32 CGKRK peptide. *Journal of Drug Targeting*. 2021; 29: 617–630.
- [18] Wang JY, Wang Y, Meng X. Chitosan Nanolayered Cisplatin-Loaded Lipid Nanoparticles for Enhanced Anticancer Efficacy in Cervical Cancer. *Nanoscale Research Letters*. 2016; 11: 524.
- [19] Kamel KM, Khalil IA, Rateb ME, Elgendy H, Elhawary S. Chitosan-Coated Cinnamon/Oregano-Loaded Solid Lipid Nanoparticles to Augment 5-Fluorouracil Cytotoxicity for Colorectal Cancer: Extract Standardization, Nanoparticle Opti-

- mization, and Cytotoxicity Evaluation. *Journal of Agricultural and Food Chemistry*. 2017; 65: 7966–7981.
- [20] Honary S, Zahir F. Effect of zeta potential on the properties of nano-drug delivery systems-a review (Part 2). *Tropical Journal of Pharmaceutical Research*. 2013; 12: 265–273.
- [21] Faal Maleki M, Jafari A, Mirhadi E, Askarizadeh A, Golichenari B, Hadizadeh F, *et al.* Endogenous stimuli-responsive linkers in nanoliposomal systems for cancer drug targeting. *International Journal of Pharmaceutics*. 2019; 572: 118716.
- [22] Senthil Kumar C, Thangam R, Mary SA, Kannan PR, Arun G, Madhan B. Targeted delivery and apoptosis induction of trans-resveratrol-ferulic acid loaded chitosan coated folic acid conjugate solid lipid nanoparticles in colon cancer cells. *Carbohydrate Polymers*. 2020; 231: 115682.
- [23] Mashreghi M, Faal Maleki M, Askarizadeh A, Farshchi H, Farhoudi L, Nasrollahzadeh MS, *et al.* A novel and easy to prepare azo-based bioreductive linker and its application in hypoxia-sensitive cationic liposomal doxorubicin: Synthesis, characterization, *in vitro* and *in vivo* studies in mice bearing C26 tumor. *Chemistry and Physics of Lipids*. 2022; 247: 105226.
- [24] Rahmati A, Homayouni Tabrizi M, Karimi E, Zarei B. Fabrication and assessment of folic acid conjugated-chitosan modified PLGA nanoparticle for delivery of alpha terpineol in colon cancer. *Journal of Biomaterials Science. Polymer Edition*. 2022; 33: 1289–1307.
- [25] Askarizadeh A, Mashreghi M, Mirhadi E, Mirzavi F, Shargh VH, Badiie A, *et al.* Doxorubicin-loaded liposomes surface engineered with the matrix metalloproteinase-2 cleavable polyethylene glycol conjugate for cancer therapy. *Cancer Nanotechnology*. 2023; 14: 18.
- [26] Haider M, Abdin SM, Kamal L, Orive G. Nanostructured Lipid Carriers for Delivery of Chemotherapeutics: A Review. *Pharmaceutics*. 2020; 12: 288.
- [27] Abdellatif AAH, Alhumaydhi FA, Al Rugaie O, Tolba NS, Mousa AM. Topical silver nanoparticles reduced with ethylcellulose enhance skin wound healing. *European Review for Medical and Pharmacological Sciences*. 2023; 27: 744–754.
- [28] Gonzalez-Mira E, Egea MA, Souto EB, Calpena AC, García ML. Optimizing flurbiprofen-loaded NLC by central composite factorial design for ocular delivery. *Nanotechnology*. 2011; 22: 045101.
- [29] Abdellatif AAH, Alturki HNH, Tawfeek HM. Different cellulosic polymers for synthesizing silver nanoparticles with antioxidant and antibacterial activities. *Scientific Reports*. 2021; 11: 84.
- [30] Moghimi SM, Hunter AC, Andresen TL. Factors controlling nanoparticle pharmacokinetics: an integrated analysis and perspective. *Annual Review of Pharmacology and Toxicology*. 2012; 52: 481–503.
- [31] Truong NP, Whittaker MR, Mak CW, Davis TP. The importance of nanoparticle shape in cancer drug delivery. *Expert Opinion on Drug Delivery*. 2015; 12: 129–142.
- [32] Abbasalipourkabir R, Fallah M, Sedighi F, Maghsood AH, Javid S. Nanocapsulation of nitazoxanide in solid lipid nanoparticles as a new drug delivery system and *in vitro* release study. *Journal of Biological Sciences*. 2016; 16: 120–127.
- [33] Ossama M, Hathout RM, Attia DA, Mortada ND. Enhanced Allicin Cytotoxicity on HEPG-2 Cells Using Glycyrrhetic Acid Surface-Decorated Gelatin Nanoparticles. *ACS Omega*. 2019; 4: 11293–11300.
- [34] Duan Y, Dhar A, Patel C, Khimani M, Neogi S, Sharma P, *et al.* A brief review on solid lipid nanoparticles: part and parcel of contemporary drug delivery systems. *RSC Advances*. 2020; 10: 26777–26791.
- [35] Shazly GA. Ciprofloxacin Controlled-Solid Lipid Nanoparticles: Characterization, *In Vitro* Release, and Antibacterial Activity Assessment. *BioMed Research International*. 2017; 2017: 2120734.
- [36] He H, Yao J, Zhang Y, Chen Y, Wang K, Lee RJ, *et al.* Solid lipid nanoparticles as a drug delivery system to across the blood-brain barrier. *Biochemical and Biophysical Research Communications*. 2019; 519: 385–390.
- [37] Sadat Khadem F, Es-Haghi A, Homayouni Tabrizi M, Shabestarian H. The loaded Ferula assa-foetida seed essential oil in Solid lipid nanoparticles (FSEO-SLN) as the strong apoptosis inducer agents in human NTERA-2 embryocarcinoma cells. *Materials Technology*. 2022; 37: 1120–1128.
- [38] Uner M, Yener G. Importance of solid lipid nanoparticles (SLN) in various administration routes and future perspectives. *International Journal of Nanomedicine*. 2007; 2: 289–300.
- [39] Ali A, Ahmed S. A review on chitosan and its nanocomposites in drug delivery. *International Journal of Biological Macromolecules*. 2018; 109: 273–286.
- [40] M Ways TM, Lau WM, Khutoryanskiy VV. Chitosan and Its Derivatives for Application in Mucoadhesive Drug Delivery Systems. *Polymers*. 2018; 10: 267.
- [41] Lu B, Lv X, Le Y. Chitosan-Modified PLGA Nanoparticles for Control-Released Drug Delivery. *Polymers*. 2019; 11: 304.
- [42] da Rocha MCO, da Silva PB, Radicchi MA, Andrade BYG, de Oliveira JV, Venus T, *et al.* Docetaxel-loaded solid lipid nanoparticles prevent tumor growth and lung metastasis of 4T1 murine mammary carcinoma cells. *Journal of Nanobiotechnology*. 2020; 18: 43.
- [43] Jansook P, Fülöp Z, Ritthidej GC. Amphotericin B loaded solid lipid nanoparticles (SLNs) and nanostructured lipid carrier (NLCs): physicochemical and solid-solution state characterizations. *Drug Development and Industrial Pharmacy*. 2019; 45: 560–567.
- [44] Shafique M, Khan MA, Khan WS, Maqsood ur R, Ahmad W, Khan S. Fabrication, Characterization, and *In Vivo* Evaluation of Famotidine Loaded Solid Lipid Nanoparticles for Boosting Oral Bioavailability. *Journal of Nanomaterials*. 2017; 2017: 7357150.
- [45] Liu Y, Pan J, Feng SS. Nanoparticles of lipid monolayer shell and biodegradable polymer core for controlled release of paclitaxel: effects of surfactants on particles size, characteristics and *in vitro* performance. *International Journal of Pharmaceutics*. 2010; 395: 243–250.
- [46] Qureshi OS, Kim HS, Zeb A, Choi JS, Kim HS, Kwon JE, *et al.* Sustained release docetaxel-incorporated lipid nanoparticles with improved pharmacokinetics for oral and parenteral administration. *Journal of Microencapsulation*. 2017; 34: 250–261.
- [47] Nadeem MS, Kazmi I, Ullah I, Muhammad K, Anwar F. Allicin, an Antioxidant and Neuroprotective Agent, Ameliorates Cognitive Impairment. *Antioxidants (Basel, Switzerland)*. 2021; 11: 87.
- [48] Hayes JD, Dinkova-Kostova AT, Tew KD. Oxidative Stress in Cancer. *Cancer Cell*. 2020; 38: 167–197.
- [49] Barrera G, Cucci MA, Grattarola M, Dianzani C, Muzio G, Pizzimenti S. Control of Oxidative Stress in Cancer Chemoresistance: Spotlight on Nrf2 Role. *Antioxidants (Basel, Switzerland)*. 2021; 10: 510.
- [50] Melino S, Leo S, Toska Papajani V. Natural Hydrogen Sulfide Donors from *Allium* sp. as a Nutraceutical Approach in Type 2 Diabetes Prevention and Therapy. *Nutrients*. 2019; 11: 1581.
- [51] Alibolandani M, Amel Farzad S, Mohammadi M, Abnous K, Taghdisi SM, Kalalinia F, *et al.* Tetrac-decorated chitosan-coated PLGA nanoparticles as a new platform for targeted delivery of SN38. *Artificial Cells, Nanomedicine, and Biotechnology*. 2018; 46: 1003–1014.
- [52] Rajpoot K, Jain SK. Colorectal cancer-targeted delivery of oxaliplatin via folic acid-grafted solid lipid nanoparticles: preparation

- ration, optimization, and *in vitro* evaluation. *Artificial Cells, Nanomedicine, and Biotechnology*. 2018; 46: 1236–1247.
- [53] Nosrat T, Tabrizi MH, Etmnan A, Irani M, Zarei B, Rahmati A. *In Vitro* and *In Vivo* Anticancer Activity of Ferula Gummosa Essential Oil Nanoemulsions (FGEO-NE) for the Colon Cancer Treatment. *Journal of Polymers and the Environment*. 2022; 30: 4166–4177.
- [54] Chen H, Zhu B, Zhao L, Liu Y, Zhao F, Feng J, *et al.* Allicin Inhibits Proliferation and Invasion *in Vitro* and *in Vivo* via SHP-1-Mediated STAT3 Signaling in Cholangiocarcinoma. *Cellular Physiology and Biochemistry: International Journal of Experimental Cellular Physiology, Biochemistry, and Pharmacology*. 2018; 47: 641–653.
- [55] Chu YL, Ho CT, Chung JG, Raghu R, Lo YC, Sheen LY. Allicin induces anti-human liver cancer cells through the p53 gene modulating apoptosis and autophagy. *Journal of Agricultural and Food Chemistry*. 2013; 61: 9839–9848.
- [56] Mulik RS, Mönkkönen J, Juvonen RO, Mahadik KR, Paradkar AR. Apoptosis-induced anticancer effect of transferrin-conjugated solid lipid nanoparticles of curcumin. *Cancer Nanotechnology*. 2012; 3: 65–81.
- [57] Hajipour H, Hamishehkar H, Rahmati-yamchi M, Shanehbandi D, Nazari Soltan Ahmad S, Hasani A. Enhanced Anti-Cancer Capability of Ellagic Acid Using Solid Lipid Nanoparticles (SLNs). *International Journal of Cancer Management*. 2018; 11: e9402.